9. U. Johanson *et al.*, *Science* **290**, 344 (2000).
10. S. B. Sung, R. M. Amasino, *Nature* **427**, 159 (2004).
11. A. R. Gendall, Y. Y. Levy, A. Wilson, C. Dean, *Cell* **107**, 525 (2001).
12. Y. Y. Levy, S. Mesnage, J. S. Mylne, A. R. Gendall, C. Dean, *Science* **297**, 243 (2002).
13. Materials and methods are available as supporting material on *Science* Online.
14. D. Lijavetzky *et al.*, *Genome* **42**, 1176 (1999).
15. J. Putterill, F. Robson, K. Lee, R. Simon, G. Coupland, *Cell* **80**, 847 (1995).
16. F. Robson *et al.*, *Plant J.* **28**, 619 (2001).
17. S. Griffiths, R. P. Dunford, G. Coupland, D. A. Laurie, *Plant Physiol.* **131**, 1855 (2003).
18. L. Yan, A. Loukoianov, J. Dubcovsky, unpublished data.
19. S. Kurup, H. D. Jones, M. J. Holdsworth, *Plant J.* **21**, 143 (2000).
20. R. Takahashi, "Catalogue of the barley germplasm preserved in Okayama University" (Research Institute for Bioresources, Okayama University, Okayama, Japan, 1983).
21. C.-L. Chen, thesis, University of California, Davis (2002).
22. W. D. Clayton, S. A. Renvoize, *Genera Graminum: Grasses of the world* (Royal Botanic Gardens, Kew, London, 1986).
23. We thank X. Zhang, A. Sanchez, J. Lin, R. Shao, and C. S. Busso for excellent technical assistance; C. M. Leutenegger for his help with the TaqMan systems; V. Chandler for the pMCG161 vector; the U.S. National Small Grain Collection for the *T. monococcum* seeds; and Okayama University (Japan) and A. Kleinhofs for the barley seeds. Supported by the U.S. Department of Agriculture, National Research Initiative grant nos. 2000-1678 and 2003-00929, and by NSF Plant Genome Research Program no. 9975793.

Supporting Online Material
www.sciencemag.org/cgi/content/full/303/5664/1640/DC1
Materials and Methods
SOM Text
Figs. S1 to S17
Table S1
References and Notes

3 December 2003; accepted 2 February 2004

REPORTS

Elastomeric Transistor Stamps: Reversible Probing of Charge Transport in Organic Crystals

Vikram C. Sundar,[1]*† Jana Zaumseil,[1]*‡ Vitaly Podzorov,[2]* Etienne Menard,[3] Robert L. Willett,[1] Takao Someya,[1]§ Michael E. Gershenson,[2] John A. Rogers[3]‖

We introduce a method to fabricate high-performance field-effect transistors on the surface of freestanding organic single crystals. The transistors are constructed by laminating a monolithic elastomeric transistor stamp against the surface of a crystal. This method, which eliminates exposure of the fragile organic surface to the hazards of conventional processing, enables fabrication of rubrene transistors with charge carrier mobilities as high as ~15 $cm^2/V{\cdot}s$ and subthreshold slopes as low as 2 $nF{\cdot}V/decade{\cdot}cm^2$. Multiple relamination of the transistor stamp against the same crystal does not affect the transistor characteristics; we exploit this reversibility to reveal anisotropic charge transport at the basal plane of rubrene.

Basic scientific interest and potential applications in large-area, flexible electronic systems motivate research in the field of organic semiconductors (*1*–*4*). Despite a substantial body of work aimed at understanding charge transport in these materials (*5*–*11*), a well-developed, microscopic description is still lacking. It is for this reason that studies of organic single crystals, in which grain boundaries are eliminated and concentration of charge traps is minimized, are important. A primary experimental difficulty is that the field-effect structures that are needed for these measurements require fabrication steps that can disrupt molecular order and bonding, generate interfacial trapping sites, create barriers to charge injection, and cause other unwanted changes to these fragile molecular systems (*12*). There is, therefore, a strong need for nondestructive, reversible methods to fabricate field-effect transistors (FETs) based on single crystals of organic semiconductors in a way that reveals intrinsic properties and removes processing-related effects.

In our technique, the transistor circuitry (the source-drain-gate electrodes and gate dielectric) is fabricated on a flexible elastomeric substrate, which, at the final stage, is bonded to the surface of organic crystal by van der Waals forces. In this respect, our technique is similar to the fabrication of organic FETs by laminating an organic crystal against a silicon wafer with predeposited electrodes (*8*, *9*). The main advantage of both elastomeric and Si-based stamp techniques is obvious: They eliminate the need for deposition of metals and dielectrics directly onto a very fragile organic surface. The elastomeric technique, however, has two important advantages compared with the Si-based technique. First, in contrast with Si-based substrates that require very thin (~1 μm) and bendable crystals (which are prone to strain-induced defects), the elastomeric stamps are compatible with much thicker (up to a few mm) and rigid crystals, as the flexible elastomeric surface and the ductile Au contacts adjust easily to the crystal shape. Second, the elastomeric stamp technique is nondestructive and reversible. The contact between the stamp and organic crystals can be reestablished many times without affecting the transistor characteristics. We exploited this experimental capability to explore the dependence of the field-effect mobility on the orientation of the transistor channel relative to the crystallographic axes and observed for the first time a strong anisotropy of the field-effect mobility within the *a*-*b* plane of single crystals of rubrene.

Figure 1 shows the transistor stamps used and outlines the steps of device fabrication. A flexible elastomer, polydimethylsiloxane (PDMS), is used as a substrate on which the transistor stamp is constructed (*13*). Gate and source-drain electrodes (Ti/Au) are evaporated through shadow masks and are separated by an additively transferred thin film (2 to 4 μm) of PDMS (*14*). The flexibility of both the dielectric and the substrate (and therefore all the gold electrodes in these transistor stamps) enables assembly of devices through simple lamination of the organic crystal and elastomeric stamp surface (*13*). Slight pressure applied to one edge of the crystal initiates contact with the stamp (Fig. 1B); van der Waals forces then spontaneously cause a "wetting" front to proceed across the surface of the crystal (Fig. 1B, center frame). The low free-surface energy of PDMS favors the progression of such a wetting front (*15*, *16*) across the flat surfaces of organic crystals. The absence of interference fringes (as observed

[1]Bell Laboratories, Lucent Technologies, Murray Hill, NJ 07974, USA. [2]Department of Physics and Astronomy, Rutgers University, Piscataway, NJ 08854, USA. [3]Department of Materials Science and Engineering, Department of Chemistry, Beckman Institute and Seitz Materials Research Laboratory, University of Illinois, Urbana-Champaign, IL 61801, USA.

*These authors contributed equally to this work.
†Present address: IBM, Yorktown Heights, NY 10598, USA.
‡Present address: Cavendish Laboratory, Cambridge CB3 0HE, UK.
§Present address: University of Tokyo, Tokyo 264-8505, Japan.
‖To whom correspondence should be addressed. E-mail: jrogers@uiuc.edu

through a high-resolution optical microscope) suggests an atomic-scale, intimate contact of the semiconductor with the electrodes (*17*, *18*) and the elastomeric gate dielectric (*19*), consistent with the electrical measurements described below.

The ease of this assembly process and its inherently noninvasive nature enable systematic analysis of the semiconducting properties of pristine organic crystals. The present work focuses on high-purity crystals of rubrene (Fig. 2A), synthesized with a physical vapor transport technique (*6*, *20*). This material forms an orthorhombic crystal with herringbone molecular packing. Figure 2B shows the relative orientation of rubrene molecules in the basal (*a*-*b*) plane of the crystal; the lattice constants along *a* and *b* axes are 14.4 and 7.2 Å, respectively. Slower crystal growth along the *c* axis results in the formation of thin platelets, 0.2 to 1.0 mm thick and 2 to 3 mm wide, with the natural large-area flat facet being the (001) *a*-*b* plane. The FETs are built by lamination on these surfaces. Images collected through crossed polarizers indicate that the crystals grown in this fashion are single crystalline (Fig. 2C) (*21*). The natural facets of the crystals match the crystallographic directions obtained from Laue diffraction profiles (Fig. 2D).

Figure 3A shows current-voltage characteristics of a representative device (*13*). Strong field-effect modulation of the channel conductance is observed, with on/off current ratios as high as 10^6 (measured between gate voltage V_G = –100 V and 20 V). By fitting the data to linear and saturation regime standard FET equations (*22*), two-probe mobilities μ = 3 to 15 $cm^2/V{\cdot}s$ were obtained for different rubrene crystals. The highly ohmic current-voltage characteristics at low source-drain bias (Fig. 3A, inset), together with nearly equal values of the mobility extracted from the linear and saturation regimes, are consistent with a relatively low Schottky barrier to hole injection and thus low contact resistance. Transfer characteristics of such devices (fig. S1) yield subthreshold slopes ~3 to 5 V/decade [corresponding to intrinsic subthreshold slopes 2 to 4 $nF{\cdot}V/decade{\cdot}cm^2$ (*7*, *13*)] and show nearly thresholdless operation and weak gate voltage dependence of the channel mobility. Minor hystereses observed in forward and reverse scans suggest a low density of deep traps at the interface. These excellent transistor characteristics result from the high quality of the laminated rubrene-PDMS interface and the high-purity rubrene crystals.

Because the adhesion of the PDMS elastomer to the organic is driven primarily by van der Waals forces and not by irreversible bond formation, separation of the elastomeric stamp from the organic crystal does not degrade the crystal surface provided that these forces are weaker than the intermolecular bonding. This is the case for rubrene: There are no substantial changes in channel conductance even upon multiple relamination of the stamp. This reversibility is important because, unlike previous efforts (*6*–*10*), it enables different high-performance transistor structures, each with different electrode configurations, to be assembled sequentially on the same region of the crystal surface. Figure 3B shows, as an example, data collected from a set of devices with different channel lengths assembled one after another on a single small region of the crystal surface. Variations of the device characteristics (mobility, e.g.) were within 15%. As a result, the saturation current observed in Fig. 3B (inset) shows the expected width/length (W/L) scaling.

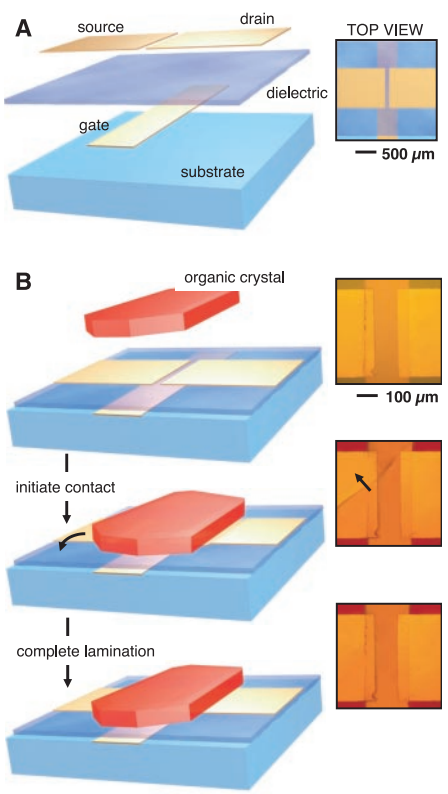

Fig. 1. (**A**) Schematic view of a transistor stamp with gate, dielectric, and source-drain electrodes sequentially deposited onto a PDMS substrate. The right inset shows a top view. (**B**) Transistor fabrication by lamination of an organic crystal against the transistor stamp. Initiating contact (first frame) between these two surfaces results in a "wetting" front that progresses across the semiconductor-stamp interface (second frame) until the entire crystal is in intimate contact with the stamp (final frame). The right insets show optical micrographs of three stages of this process. The arrow in the middle inset marks the progression of the wetting front.

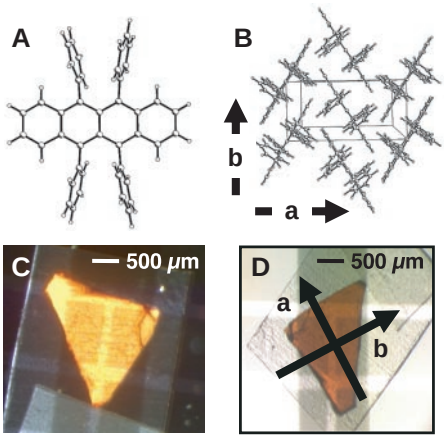

Fig. 2. (**A**) Molecular structure of rubrene. (**B**) Orthorhombic, crystallographic structure of a single crystal of rubrene shows the enhanced π-π overlap along the *b* direction and reduced overlap along the *a* direction. (**C**) Optical micrograph of a sample viewed through crossed polarizers. (**D**) Natural facets on the crystal surface correspond well to the crystallographic data and enable easy identification of the *a* and *b* axes confirmed by Laue diffraction.

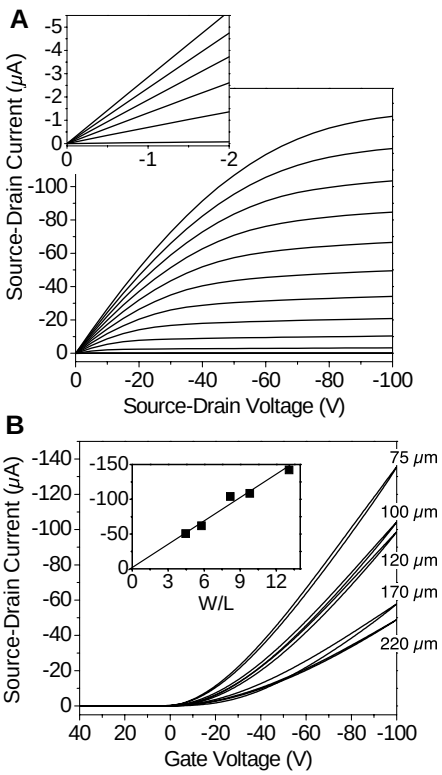

Fig. 3. (**A**) Current-voltage characteristics of laminated rubrene-transistor stamp assemblies (L = 75 μm, W = 980 μm, C_i = 0.67 nF/cm^2). Typical FET behavior, with well-resolved linear and saturation current regimes (*13*), is observed. The channel is normally "off" and turns on at successively more negative gate voltage (from +20 to –100 V). The graph in the inset shows the behavior at low V_{SD}. Highly ohmic behavior is evident at all gate voltages. (**B**) Transfer characteristics measured at V_{SD} = –100 V in the same region of one single crystal by forming, one after another, contacts with transistor stamp structures that define different channel lengths (L = 220, 170, 120, 100, and 75 μm; W = 980 μm). Similar mobilities and subthreshold slopes are seen for all devices (3.4 ± 0.3 $cm^2/V{\cdot}s$ and 2.5 ± 0.3 $nF{\cdot}V/decade{\cdot}cm^2$, respectively). As a result, the inset shows linear scaling of saturation currents with W/L.

By performing experiments with the same source-drain configuration but with different angular orientations of the crystal relative to the channel, it is possible to examine mobility anisotropy. Figure 4A presents results of such measurements, in which the crystal was rotated and relaminated through 720° in a stepwise fashion (*13*). After each rotation, the two-probe mobility was measured in both linear and saturation regime to exclude the contact effects (*13*). Reproducibility of the results after two full 360° rotations demonstrates that relamination does not damage the crystal surface. The effective two-probe mobilities for charge transport along the crystallographic *a* and *b* axes differ at least by a factor of two, with the highest mobility along the *b* axis. The angular dependence of the mobility variation is consistent with tensor transformation rules for an orthorhombic crystal (Fig. 4A, dashed line) (*23*). All investigated samples showed similar behavior (six samples taken from different crystal and transistor stamp syntheses) and highlighted the noninvasive nature of this technique.

To eliminate entirely the effects of contacts and to extract intrinsic hole mobilities, we used stamps with a four-probe configuration of electrodes (Fig. 4B, inset) (*6*, *7*, *22*). In this experiment, the potential difference between two voltage contacts located inside the channel, V_{4W}, was measured as a function of gate voltage simultaneously with the source-drain current, I_{SD}. The conductivity, $\sigma = I_{SD}/V_{4W}$, is plotted as a function of V_G for the transport along the *a* and *b* crystallographic directions (Fig. 4B). The slope of the $\sigma(V_G)$ dependences in the linear regime is proportional to the intrinsic hole mobility μ_{4W} in rubrene (*22*, *24*). Again, this mobility is dramatically different along the *a* and *b* axes (4.4 $cm^2/V{\cdot}s$ and 15.4 $cm^2/V{\cdot}s$, respectively). Contact resistance (*25*) extracted from these data (Fig. 4B, inset) varies with V_G in a similar fashion along both crystallographic directions. These results show that the observed mobility anisotropy in the two-probe measurements indeed reflects the specific crystal structure.

Although it is known that organic single crystals are highly anisotropic (*5*), manifestations of these effects in field-effect experiments have not been previously reported. Our observation that the maximum mobility is realized for hole transport along the *b* axis is qualitatively consistent with molecular packing in the rubrene crystal (Fig. 2A), for which one might expect a stronger overlap of the electronic π orbitals along the *b* axis (Fig. 2B). The different lattice constants along the *a* and *b* axes (14.4 Å versus 7.2 Å) and the anisotropic character of inter- and intramolecular vibrational modes are also likely to contribute to the observed anisotropy. Qualitatively, our finding agrees with the theoretically predicted mobility anisotropy in molecular crystals based on differences in transfer integrals along different crystallographic axes (*26*); however, for a more quantitative analysis, polaronic effects in rubrene and other polyacenes should be included (*27*).

These results suggest that future field-effect experiments at organic crystal surfaces should consider mobility anisotropy and highlight the importance of controlling the orientation of the organic crystal relative to the FET channel. More broadly, the reversible lamination of transistor stamps demonstrated in this report provides simple two- and four-probe stamps that could be effectively used to extract spatial channel characteristics in a single grain, as well as across the grain boundary of organic semiconductors (*28*). The reversible formation of the interface between the PDMS dielectrics and organic surface allows for a reliable interpretation of these results and enables a better understanding of charge transport in organic semiconductor. More generally, this technique could facilitate studies of operation-induced changes in transport properties by providing direct access to interfaces that are irreversibly embedded in conventional devices.

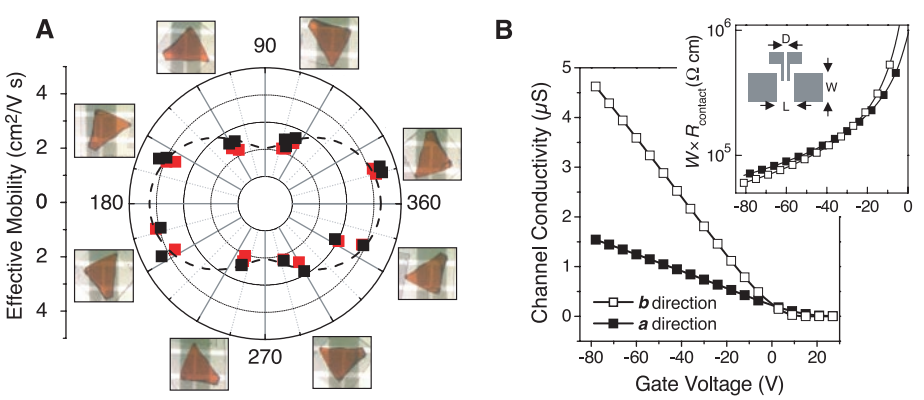

Fig. 4. (**A**) Polar plot of the mobility at the rubrene *a*-*b* surface (angle measured between the *b* axis and the conducting channel). The linear and saturation mobilities (black and red squares, respectively) are similar and are seen to be coincident after each full 360° rotation. The maximum and minimum mobility values occur along the *b* (180° and 360°) and *a* (90° and 270°) axes, respectively. The dotted line shows the fitted in-plane transformation of the mobility tensor. (**B**) Four-probe conductivity as a function of gate voltage along the *b* and *a* axes. Intrinsic mobilities measured along the *b* and *a* axes are 15.4 $cm^2/V{\cdot}s$ and 4.4 $cm^2/V{\cdot}s$, respectively (*24*). The inset plots the contact resistance along the *a* and *b* directions (*25*).

References and Notes

1. J. A. Rogers, *Science* **291**, 1502 (2001).
2. H. Sirringhaus *et al.*, *Science* **290**, 2123 (2000).
3. H. E. Katz, A. Dodabalapur, Z. Bao, *Oligo- and Polythiophene-Based Field-Effect Transistors* (Wiley-WCH, Weinheim, 1998).
4. S. F. Nelson, Y.-Y. Lin, D. J. Gundlach, T. N. Jackson, *Appl. Phys. Lett.* **72**, 1854 (1998).
5. M. Pope, C. Swenberg, *Electronic Processes in Organic Crystals and Polymers* (Oxford Univ. Press, Oxford, 1999).
6. V. Podzorov, V. M. Pudalov, M. E. Gershenson, *Appl. Phys. Lett.* **82**, 1739 (2003).
7. V. Podzorov, S. E. Sysoev, E. Loginova, V. M. Pudalov, M. E. Gershenson, *Appl. Phys. Lett.* **83**, 3504 (2003).
8. R. W. I. De Boer, T. M. Klapwijk, A. F. Morpurgo, *Appl. Phys. Lett.* **83**, 4345 (2003).
9. J. Takeya *et al.*, *J. Appl. Phys.* **94**, 5800 (2003).
10. V. Y. Butko, X. Chi, D. V. Lang, A. P. Ramirez, *Appl. Phys. Lett.* **83**, 4773 (2003).
11. D. J. Gundlach, J. A. Nichols, L. Zhou, T. N. Jackson, *Appl. Phys. Lett.* **80**, 2925 (2002).
12. G. Horowitz, *Adv. Mater.* **10**, 365 (1998).
13. Materials and methods are available as supporting material on *Science* Online.
14. W. R. Childs, R. G. Nuzzo, *J. Am. Chem. Soc.* **124**, 13583 (2002).
15. S. Perutz, J. Wang, E. J. Kramer, C. K. Ober, K. Ellis, *Macromolecules* **31**, 4272 (1998).
16. D. Hull, *Introduction to Composite Materials* (Cambridge Univ. Press, Cambridge, 1981).
17. Y.-L. Loo *et al.*, *Proc. Natl. Acad. Sci. U.S.A.* **99**, 10252 (2002).
18. J. Zaumseil, K. W. Baldwin, J. A. Rogers, *J. Appl. Phys.* **93**, 6117 (2003).
19. H. O. Jacobs, G. M. Whitesides, *Science* **291**, 1763 (2001).
20. R. A. Laudise, Ch. Kloc, P. G. Simpkins, T. Siegrist, *J. Cryst. Growth* **187**, 449 (1998).
21. J. Vrijmoeth, R. W. Stok, R. Veldman, W. A. Schoonveld, T. M. Klapwijk, *J. Appl. Phys.* **83**, 3816 (1998).
22. S. M. Sze, *Physics of Semiconductor Devices* (Wiley, New York, 1981).
23. A. C. Smith, J. F. Janak, R. B. Adler, *Electrical Conduction in Solids* (McGraw-Hill, New York, 1967), p. 257.
24. Intrinsic hole mobility $\mu_{4W} = (D/WC_i)(d\sigma/dV_G)$, where D is the distance between the voltage probes, W is the channel width, C_i is the capacitance of the gate dielectric, and d is the derivative operator.
25. $R_{contact} = (V_{SD}/I_{SD}) - (L/D)(V_{4W}/I_{SD})$.
26. Y. C. Cheng *et al.*, *J. Chem. Phys.* **118**, 3764 (2003).
27. M. W. Wu, E. M. Conwell, *Chem. Phys. Lett.* **266**, 363 (1997).
28. A. B. Chwang, C. D. Frisbie, *J. Appl. Phys.* **90**, 1342 (2001).

29. V.P. and M.E.G. were supported by NSF grant DMR-0077825. Atomic force microscopy measurements were done in the Center for Microanalysis of Materials at the University of Illinois, Urbana-Champaign (partially funded by U.S. Department of Energy grant DEFG02-91-ER45439). We thank A. Erbe, Y.-L. Loo, K. W. Baldwin, C. Kloc, A. Borissov, V. Kiryukhin, M. Watson, and A. Shim (Dow Corning) for technical support and helpful discussions.

Supporting Online Material

www.sciencemag.org/cgi/content/full/303/5664/1644/DC1
Materials and Methods
Fig. S1

1 December 2003; accepted 9 February 2004